JOURNAL OF MATERIALS SCIENCE 29 (1994) 5826–5832

Development of Al–Mg–Li alloys for marine applications

L. S. KRAMER, T. J. LANGAN, J. R. PICKENS
Martin Marietta Laboratories, Baltimore, MD 21227, USA

H. LAST
Naval Surface Warfare Center, Silver Spring, MD 20903, USA

Based on the promising properties of a family of Al–Mg–Li alloys known as Weldalite® 050 alloys, a series of experimental variants were fabricated and evaluated. After being cast, extruded into rectangular bars, and heat treated, a series of mechanical tests was performed to select a composition for marine applications. The alloy variant selected as the most promising candidate displays tensile properties of 438 MPa yield strength, 543 MPa ultimate tensile strength, 5% elongation and 79 GPa elastic modulus, with excellent corrosion and stress corrosion cracking resistance at a density of 2.51 g cm^{-3}.

1. Introduction

The alloying of aluminium with lithium is a very effective way to decrease density and increase modulus. The lithium-containing aluminium ingot metallurgy (I/M) alloys that have been commercialized in the West are almost exclusively based on the Al–Cu–Li or Al–Cu–Li–Mg systems. For these alloys, copper-containing precipitates impart high strengths, as demonstrated in the very high-strength Weldalite® 049-type alloys that are primarily strengthened by fine $T_1(Al_2CuLi)$ plateletes [1]. Unfortunately, copper-containing aluminium–lithium alloys usually exhibit poor corrosion resistance in marine applications. Alloys based on the Al–Mg–Li system, such as 1420 which was developed in the Soviet Union in the 1960s, have excellent corrosion resistance, similar to that of the work-hardenable 5XXX alloys, but have increased strength due to precipitation hardening. The precipitation ageing sequence for aluminium-rich Al–Mg–Li alloys is [2, 3]

$$\text{supersaturated solid solution} \rightarrow \delta'(Al_3Li) \rightarrow Al_2MgLi$$

in which Al_2MgLi has typically been found to occur rather than δ(AlLi), as is the case for the binary Al–Li alloys. As in the 5XXX alloys, magnesium is a very effective solid-solution strengthener and reduces the solubility of lithium in aluminium resulting in the precipitation of greater amounts of δ′ [2, 4]. Equilibrium phases, such as δ(AlLi) and $Mg_{17}Al_{12}$, which do not contribute to strengthening, may also form under certain conditions [5, 6].

The Al_2MgLi phase (other stoichiometries have also been proposed) was originally thought to contribute to strengthening [7]. However, this phase forms as coarsely dispersed rods [3] or on grain boundaries [4] and tends to inhibit deformation in grain-boundary regions thereby lowering ductility [4]. Al_2MgLi is usually found in alloys containing greater than 4% Mg or in the overaged condition. By consuming nearby δ′, Al_2MgLi prevents the formation of δ, a phase which is even more deleterious to both mechanical properties and corrosion resistance [3].

Dispersoid-forming quaternary additions to Al–Mg–Li alloys such as titanium and zirconium can be added for grain refinement and/or recrystallization inhibition. When added to increase strength, other quaternary elements may also result in a substantial ductility penalty as was found with copper additions [8]. Recently Al–Mg–Li alloys with additions of silver or zinc [9], and scandium [10, 11] have been shown to have improved strength without a significant loss in ductility. The mechanisms by which these additions improve properties are varied and in some cases not well understood, but δ′ precipitation may be influenced by changing the lithium solubility [12] or by possibly affecting the work-hardening response of the alloys. Alternatively, additional strengthening precipitates may form as was found when silver, beryllium or cadmium was added to Al–Mg alloys [13]. Polmear [14] found that age hardening, which is not a strengthening mechanism for practical Al–Mg alloys, occurs with silver additions either by raising the GP zone solvus or increasing the supersation of magnesium in the α–Al matrix.

2. Materials

Permanent mould billets, 18 kg in weight were cast, homogenized and extruded into 51 mm × 19 mm rectangular bars. The nominal extrusion parameters were a 370 °C billet preheat temperature with a 2.5 mm/s^{-1} ram speed at a ratio of 20:1. The nominal

0022–2461

TABLE I Measured experimental alloy compositions from extruded bar from the inductively coupled plasma method, wt %, bal. = Al)

Nominal Mg–Li	Mg	Li	Ag	Zr	Ti
2.8–2.6	2.68	2.55	0.36	0.13	0.03
4.0–2.3	3.78	2.24	0.40	0.14	0.03
5.0–2.0	5.14	1.99	0.35	0.13	0.03

compositions and chemical analyses of the extruded bars are given in Table I. Three compositions were selected to span the aluminium-rich corner of the ternary phase diagram so that the equilibrium phases would be different for each alloy. The aluminium corner of an isothermal section of the ternary Al–Mg–Li equilibrium phase diagram at 204 °C, with the magnesium and lithium contents of the experimental alloys superimposed on it, is shown in Fig. 1. The alloy variant containing Al–2.8 Mg–2.6 Li lies within the Al + Al_2MgLi + AlLi phase field, with the lithium content selected based on the maximum practical amount to produce commercial-scale direct chill-cast ingots. The Al–5.0 Mg–2.0 Li alloy variant is close to, or in the Al + Al_2MgLi + $Al_{12}Mg_{17}$ phase field, and was selected based on alloy 1420. The Al–4.0 Mg–2.3 Li alloy variant lies in the adjacent, AlLi-free phase field. Silver was added based on earlier work [9]. The alloys will hereafter be referred to as 2.8–2.6, 4.0–2.3, and 5.0–2.0.

Each of the billets extruded readily, and the appearance of the extruded bars was good, except that the 5.0–2.0 variant exhibited minor surface cracking near the tail. The bars were held at 468 °C for 1.25 h after heating for 1 h; at this solution heat-treatment temperature, each of the alloy variants is composed of a single (α-Al solid solution) phase. The bars were then quenched rapidly, nose first, in a water–ethylene glycol bath. Approximately 2 m was cut off from the nose of each bar in this condition, and the remaining portion was stretched approximately 5% within 90 min of the quench.

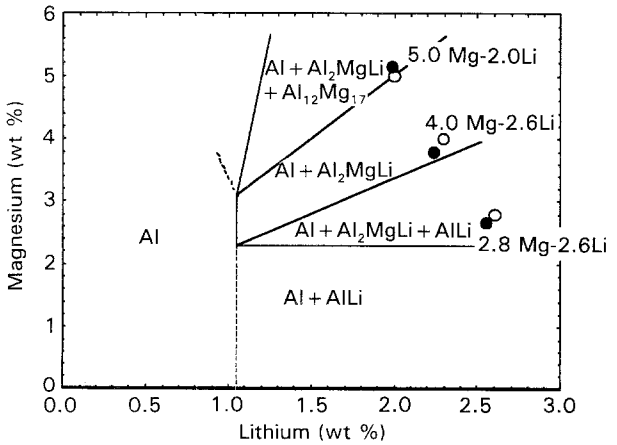

Figure 1 The published Al–Mg–Li phase diagram [8], at 204 °C with the experimental alloys superimposed on it. (○) Nominal and (●) measured compositions.

3. Experimental procedure

The Archimedes method was used to measure density. Young's modulus, E, measurements were made using ultrasonic techniques (ASTM E494).

Optimum heat-treating parameters for each of the extruded bars in the 0% and 5% stretch conditions were determined using several steps. First, isochronal (24 h) Rockwell B hardness versus ageing time curves were generated over the temperature range 125–190 °C. This enabled us to select the temperature at which peak hardness could be attained in a commercially practical time period. Tensile properties were evaluated after ageing near the peak hardness at the selected temperature. Based on the strength and elongation values of these tests, additional tensile testing was performed at different time–temperature combinations to locate the peak-aged condition, and to develop a slightly underaged condition that was designated as the T8 temper for stretched material, and the T6 temper for unstretched material.

Tensile properties were evaluated in the longitudinal (L) and long-transverse (LT) orientation in accordance with ASTM E-8. Short-transverse (ST) properties were also evaluated, although non-standard specimens were utilized. The fracture toughness of each extruded bar was measured in the LT orientation by the use of compact tension (CT) specimens in accordance with ASTM E-399. In addition, the notched tensile properties of selected specimens were evaluated.

The corrosion resistance of each alloy was evaluated by constant immersion testing (ASTM G1 and G31) in an aerated 3.5% NaCl aqueous solution. The corrosion rate was then recorded after a 90 day exposure.

Constant-strain time-to-failure (ttf) rigs were used to evaluate the stress corrosion cracking (SCC) susceptibility of the alloys. These specimens were exposed under alternate immersion (AI) (10 min wet, 50 min dry) in a 3.5% NaCl aqueous solution. Both T6 and T8 specimens were tested using standard specimens in the LT orientation, and T8 specimens were used for the non-standard ST tests. Specimens were loaded to approximately 75% of the yield strength; the target stress for the LT specimens was 39×10^3 p.s.i. (269 MPa) (T8), 38×10^3 p.s.i. (262 MPa) (T6), and 37×10^3 p.s.i. (255 MPa) for the ST (T8). Although the SCC testing complies with ASTM G44, G47, G49, and G64, there is no standard test duration for lithium-containing aluminium alloys. The LT specimens were run for 90 days, which is the longest duration stated in the standards, and much longer than the typical 40 day exposure used for some other aluminium alloy systems. Similarly, the ST tests were run for a 20 day duration.

The microstructures of selected alloys were characterized using optical metallography and transmission electron microscopy (TEM).

Differential scanning calorimetry (DSC) measurements were taken to investigate the precipitation sequence in these alloys. In these particular tests, the specimens were heated at 10 °C min^{-1} from ambient to 500 °C under flowing argon.

4. Results and discussion

4.1. Density and modulus

The density values for the alloy variants all fall within a narrow range, 2.50–2.51 g cm^{-3}. These values are significantly lower than those observed for other aluminium alloys used for marine applications such as 6061 (2.70 g cm^{-3}) or 5456 (2.66 g cm^{-3}). Young's modulus, measured in the LT orientation, increases with lithium content with values of 78 GPa for the 5.0–2.0 alloy, 79 GPa for the 4.0–2.3 alloy, and 80 GPa for the 2.8–2.6 alloy. These values are similar to those reported for other Al–Mg–Li alloys [15–17], and are significantly higher than those of 6061 (69 GPa) or 5456 (71 GPa).

4.2. Hardness

The results from hardness tests after both the stretched and unstretched specimens were artificially aged for 24 h were used to make isochronal ageing curves (Fig. 2). Many of the curves have a similar shape; that is, the highest hardness values occur over the temperature range 140–175 °C, where the curve is relatively flat, and drops off at temperatures lower and higher than this regime. The shapes of these curves enabled us easily to select an ageing temperature to produce a T6 or T8 temper.

4.3. Tensile testing

Table II gives the tensile properties obtained for the T6 and T8 artificial ageing conditions. For each alloy, the T6 condition required ageing at 160 °C for 24 h, while the T8 was attained after ageing at 143 °C for 16 h (24 h for the 5.0–2.0 alloy). These are slightly underaged tempers for each alloy, except for the 2.8–2.6 alloy, which had to be significantly underaged to attain elongations near 5%. When aged to peak-strength conditions, specimens displayed yield strengths up to 425 MPa (0% stretch), and 481 MPa (5% stretch). Note that each value is higher than those of alloys 1420(Al–5.0 Mg–2.0 Li–0.14 Zr) or 1421 (1420 + Sc) which have reported L-orientation yield strengths ranging from 290–360 MPa [10, 11], although our earlier studies indicated that higher strengths can be attained in 1420-type alloys [18].

Stretching increases yield strength while decreasing elongation probably due to the induced cold work. It is unlikely that the dislocations introduced by the stretch are serving as effective nucleation sites as they do in Al–Cu–Li alloys, because the major strengthening precipitate, δ′, nucleates homogeneously. All tensile specimens exhibited serrated yielding, which is typical of magnesium-containing aluminium alloys. Plastic deformation occurred uniformly with no necking accompanying fracture, and the fracture surfaces varied from flat with shear lips to a 45° shear mode, with no significant differences between T6 and T8 specimens. In general, the 5.0–2.0 alloy exhibited primarily flat, ragged fracture surfaces, while the 2.8–2.6 alloy occasionally exhibited step-like, or delaminated fracture surfaces. Although strength in the LT orientation is slightly lower than the L orientation, the values reported are good considering the small aspect ratio of the extruded bars.

TABLE II Tensile properties (duplicate specimens)

Alloy	Orientation	T6			T8		
		YS (MPa)	UTS (MPa)	Elongation (%)	YS (MPa)	UTS (MPa)	Elongation (%)
2.8–2.6	L	402	532	5.7	448	525	2.8
	LT	339	505	6.0	365	519	5.8
	ST				339	450	2.1
4.0–2.3	L	394	527	8.7	438	543	5.1
	LT	336	499	7.8	370	521	9.0
	ST				336	461	2.8
5.0–2.0	L	393	543	10.1	406	546	8.4
	LT	356	501	6.8	365	523	7.8
	ST				340	400[a]	1.3[a]

[a] One test.

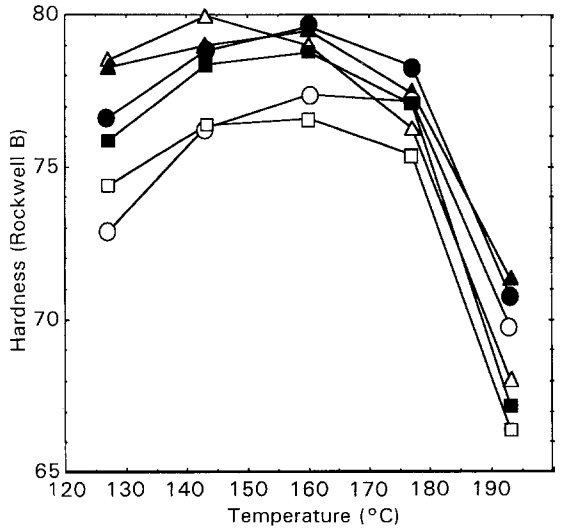

Figure 2 Isochronal (24 h) hardness curves of the experimental Mg–Al alloys: (○, ●) 2.8–2.6, (□, ■) 4.0–2.3, (▲, △) 5.0–2.0 for (○, □, △) no stretching, (●, ■, ▲) 5% stretching.

4.4. Toughness

Adequate fracture toughness is evident by the K_Q values shown in Table III, and the good NTS/YS (notched UTS: unnotched YS) ratios of the alloys tested. The 4.0–2.3 variant has a better combination of fracture toughness and YS than do the other variants, and the NTS/YS is slightly better in the T6 than the T8.

TABLE III Fracture toughness (duplicate L, LT specimens)

Alloy	Temper	K_Q (MPa m$^{1/2}$)	YS (MPa)	NTS (MPa)	NTS/YS
2.8–2.6	T8	23.7	448	499	1.11
	T6		402	504	1.25
4.0–2.3	T8	29.8	438	542	1.24
	T6		394	519	1.32
5.0–2.0	T8	22.7	406		

Different amounts of what appears to be delamination were evident on each of the fractured CT specimens. The fracture surfaces of the CT specimens of the 5.0–2.0 variant follow a straight path, whereas the 2.8–2.6 variant specimens fracture along a more tortuous path, with some specimens exhibiting a 90° turn in crack path. The crack front being diverted 90° into the extrusion direction has been reported for Al–Mg–Li toughness specimens, with K_Q values as high as 41.7 MPa $m^{1/2}$ demonstrated [8], while others have found that toughness measurements of these types of alloys could be 25% lower than true K_{1C} values [19]. Consequently, the fracture toughness measured for these alloys is probably representative. Furthermore, toughness values of 22–30 MPa $m^{1/2}$ at YS levels greater than 400 MPa is attractive for such low-density alloys.

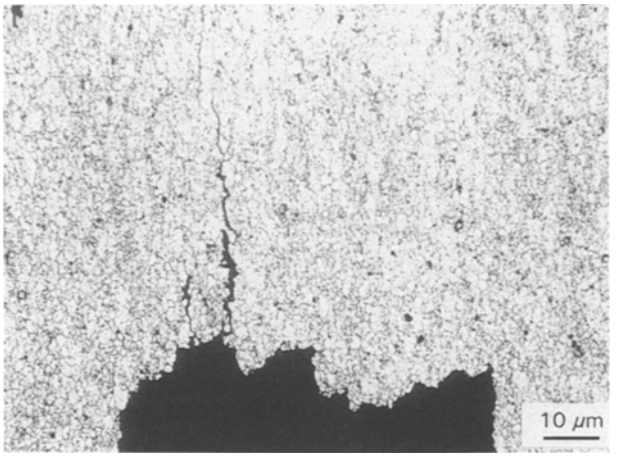

Figure 3 Intergranular crack observed on section perpendicular to the fracture surface of a ttf specimen (5.0–2.0).

4.5. Corrosion

Each alloy exhibits a very low corrosion rate over the 90 day constant immersion test (Table IV). The test coupons show virtually no evidence of corrosion, and most are indistinguishable from unexposed coupons. The results indicate that the corrosion resistance of each Weldalite® 050 variant is far superior to corrosion-resistant marine alloy 5456–H111 and alloy 7039–T6 that have been tested under identical conditions.

4.6. Stress corrosion cracking

As reported in Table V, no failures of any of the 2.8–2.6 or 4.0–2.3 alloy specimens occurred, while several of the 5.0–2.0 alloy specimens (similar to the Soviet alloy 1420) failed after only short exposures. Microstructurally, the presence of secondary intergranular cracking emanating from the fracture surface of a failed 5.0–2.0 alloy specimen (Fig. 3) suggests that failure was by SCC and not a pitting overload mechanism. Passing this accelerated test usually signifies a very high SCC resistance and an expectation of no SCC failures in service, although corresponding standard atmospheric exposure data for Al–Li alloys are not yet available. It may be that this test is quite severe for Al–Li alloys because there are no reported SCC failures of 1420 in service, although laboratory SCC test failures have been reported [20].

The mechanism of SCC in 1420-type alloys is not well understood, and has not been extensively documented. The "good" SCC resistance of 1420 has been attributed to the presence of the ternary Al_2MgLi phase on grain boundaries, which inhibits formation of the highly corrosion-susceptible δ (AlLi) phase [20, 21]. It may be that any boundary phase formation can cause corrosion or SCC susceptibility in the Al–Mg–Li system; therefore, the most corrosion-resistant alloys will contain lower amounts of solute and be used in an underaged (and certainly not overaged) condition. Furthermore, because Al_2MgLi was found to be less detrimental to corrosion resistance than δ, it is safer to select alloys in the δ-free phase field to reduce the risk of corrosion and SCC problems that might arise from improper thermomechanical processing.

TABLE IV General corrosion[a] (T8) compared with conventional alloys

	Alloy				
	2.8–2.6	4.0–2.3	5.0–2.0	5456–H111	7039–T6
Corrosion rate (μm y^{-1})	3.0	3.2	2.1	9.1	26.4

[a] Triplicate specimens.

TABLE V SCC time-to-failure tests

Alloy	Orientation	T6		T8	
		Failures/ number tested	Time to failure days	Failures/ number tested	Time to failure days
2.8–2.6	LT	0/3	NF[a]	0/3	NF
	ST			0/3	NF
4.0–2.3	LT	0/3	NF	0/3	NF
	ST			0/3	NF
5.0–2.0	LT	3/3	2,2,2	3/3	1,1,4
	ST			3/3	1,1, 1,1,11

[a] NF = no failures after 90 days (LT), or 20 days (ST).

4.7. Microscopy

The 2.8–2.6 alloy is strengthened by precipitation of fine δ′ precipitates (Fig. 4). In addition, composite "doughnut-type" $Al_3(Li, Zr)$ precipitates are also present. The magnesium probably remains in solid solution but may have some solubility in δ′ [4, 12]. Reflections other than those at the superlattice positions are not present on selected-area diffraction (SAD) patterns, and diffraction from additional precipitate phases, such as the complex "T" phase found by Polmear [14] in Al–Mg alloys when silver was

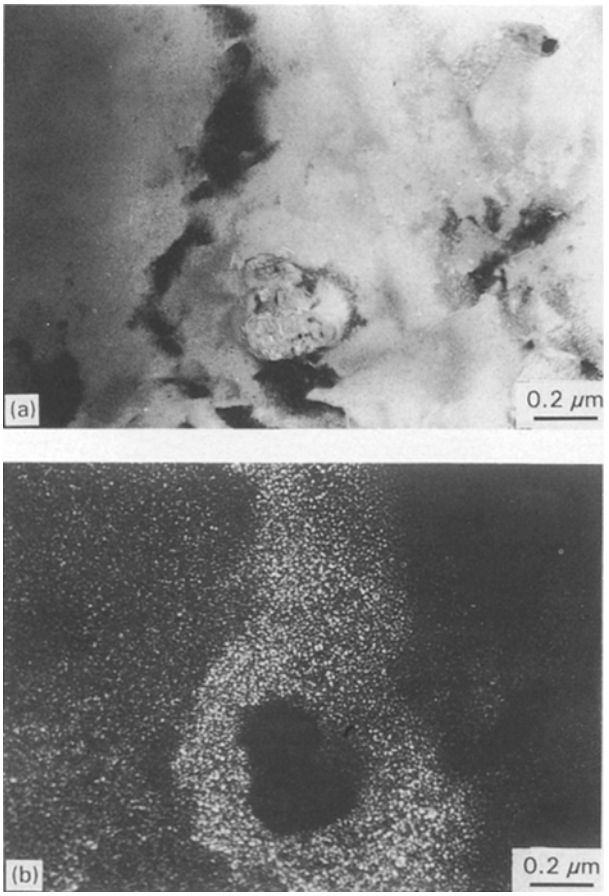

Figure 4 (a) Bright-field and (b) dark-field transmission electron micrographs of the 2.8–2.6 alloy (T8) showing δ′ precipitates.

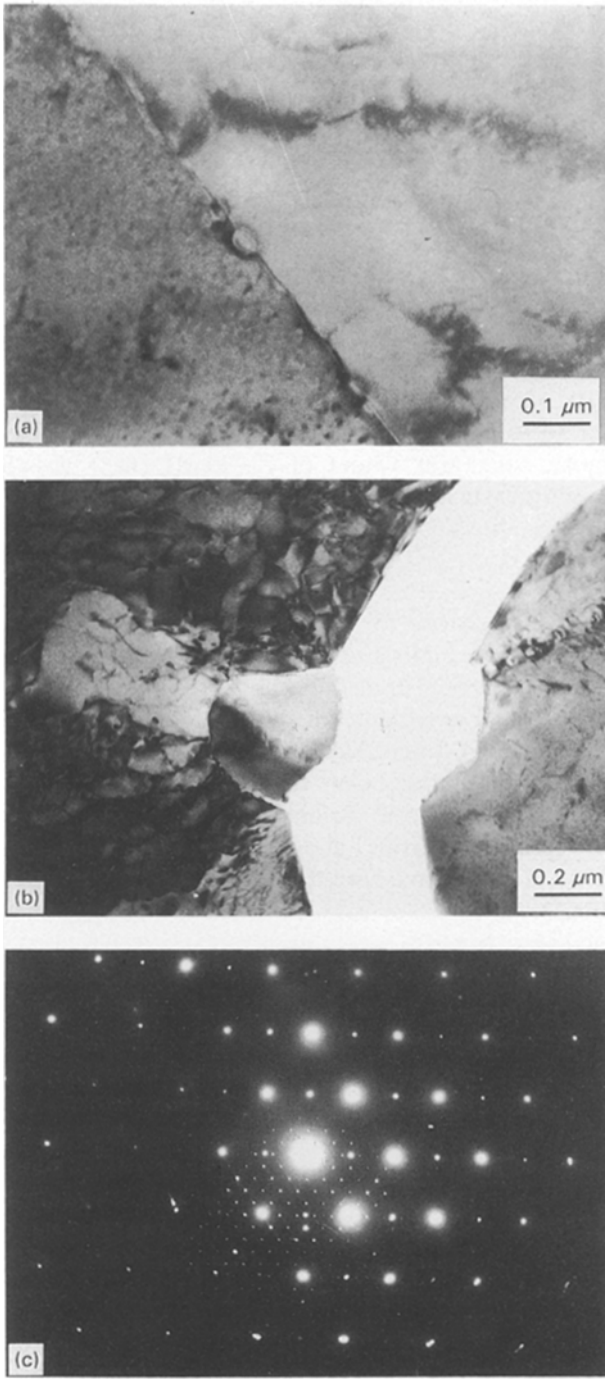

Figure 5 Transmission electron micrographs showing (a) fine grain-boundary-precipitates, and (b) Al_2MgLi boundary precipitate in the 5.0–2.0 alloy (T8) with (c) associated SADP.

added, was not observed for the 2.8–2.6 alloy. The 5.0–2.0 and 4.0–2.3 alloys are also primarily strengthened by δ′ precipitates. Thus, increasing the Mg/Li ratio moves the composition into a different phase field on the equilibrium phase diagram but does not change the metastable strengthening phase.

The small boundary precipitates with strain fields that are observed (Fig. 5a) in each of the alloy variants are similar to those observed in 1420 that were associated with Al_2MgLi precipitates [20]. Larger boundary precipitates are also present in each variant and the reflections from one such precipitate in the 5.0–2.0 alloy (Fig. 5b and c) match the structure for the Al_2MgLi phase [3]. No significant precipitate-free zone (PFZ) was observed around the large Al_2MgLi precipitates or along the grain boundaries (Fig. 6). This is most probably due to the underaged condition of the alloy.

4.8. Calorimetry

The peaks of the DSC thermograms indicate the precipitation sequence, with each alloy following a similar pattern. One endothermic peak, labelled A, and two exothermic peaks, labelled B and C, are evident in the representative scan of Fig. 7. The endothermic peak, A, which occurs slightly above 100 °C, may be attributed to the dissolution of very fine δ′ precipitates that are present in the naturally aged specimens. This is followed by the exothermic peak B, which is attributed to δ′ precipitation [5, 22]. The second exothermic peak, C, can probably be attributed to the precipitation of equilibrium Al_2MgLi. These reactions are in agreement with published Al–Mg–Li calorimetry and follow the accepted precipitation sequence [2, 5, 7, 22, 23]. Although the δ′ peaks occur at the same temperature in each of the variants tested, the Al_2MgLi peaks occur at approximately 260 °C for 2.8–2.6, 245 °C for 4.0–2.3, and 230 °C for 5.0–2.0 with the shift to lower temperatures likely related to the increase in magnesium content. The sequence of events in the DSC thermograms generated from unstretched specimens is very similar to those of the stretched specimens, which implies that cold work

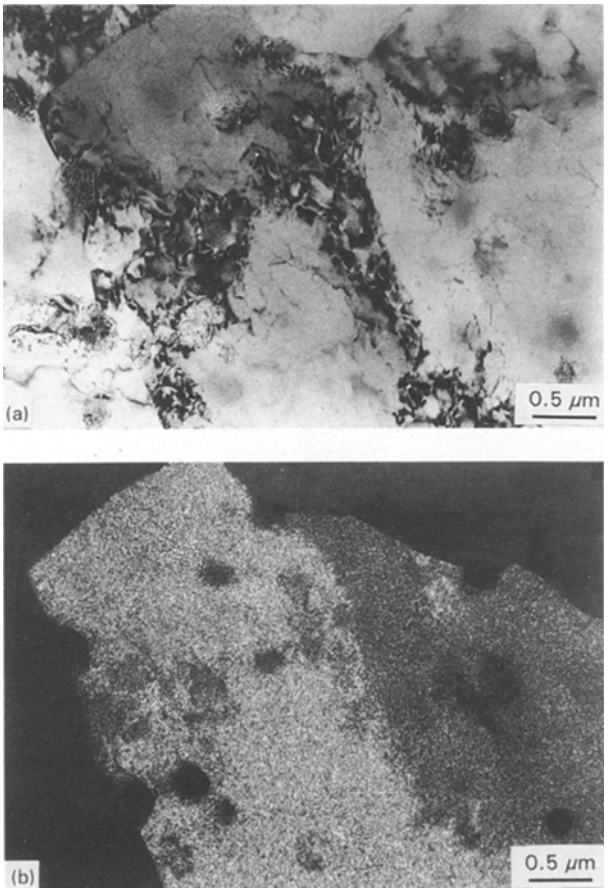

Figure 6 (a) Bright-field and (b) dark-field transmission electron micrographs of the 2.8–2.6 alloy (T8) showing no PFZ around precipitates or boundaries.

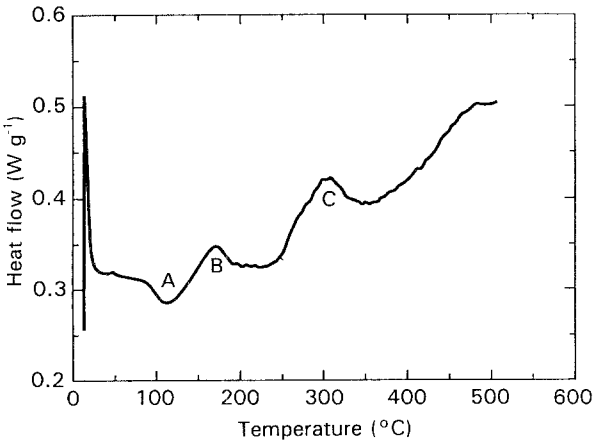

Figure 7 DSC curve of the 4.0–2.3 alloy–stretched.

increases strength mainly by work hardening rather than by affecting the precipitation sequence.

5. Conclusions

Of the three Al–Mg–Li alloys examined, the 4.0–2.3 variant exhibits the best combination of properties. The 2.8–2.6 alloy exhibits higher strengths, although elongation and toughness values are lower, while the 5.0–2.0 alloy displayed significant SCC susceptibility. Thus, we recommend that the preferred composition for marine applications is Al–4.0 Mg–2.3 Li–0.4 Ag–0.14 Zr. The properties of this alloy include a 438 MPa yield strength (YS), 543 MPa ultimate tensile strength (UTS), 5% elongation and 79 GPa elastic modulus, with corrosion resistance superior to that of 6061–T6 at a density of 2.51 $g\,cm^{-3}$. The unique combination of high strength, low density, high stiffness, and excellent corrosion resistance makes this alloy a suitable candidate for a wide variety of applications.

Acknowledgements

This research was funded by the Office of Naval Technology through Dr William Messick, the Weapons and Spacecraft Materials Block Program Manager at NSWC on contract number N60921-91-C-0193. The authors thank John Tydings, contract monitor, for his helpful discussions throughout the investigation.

References

1. T. J. LANGAN and J. R. PICKENS, in "Proceedings of the 5th International Conference on Al–Li Alloys", edited by T. H. Sanders and E. A. Starke (MCE, Birmingham, UK, 1989) p. 691.
2. T. H. SANDERS Jr and E. A. STARKE Jr (eds), Proceedings of the 2nd International Conference on Al–Li Alloys", (AIME, Warrendale, PA, 1983) p. 1.
3. G. E. THOMPSON and B. NOBLE *J. Inst. Metals* **101** (1973) 111.
4. K. DINSDALE, S. J. HARRIS and B. NOBLE, in "Proceedings of the 1st International Conference on Al–Li Alloys", edited by T. H. Sanders and E. A. Starke (AIME, 1981) p. 101.
5. H. H. JO, T. OHSHIMA and K. HIRANO, *J. Jpn Inst. Light Met.* **36** (1986) 759.
6. I. N. FRIDLYANDER, V. F. SHAMRAY and N. V. SHIRYAYEVA, *Russ. Met.* **2** (1965) 83.
7. I. N. FRIDLYANDER, V. S. SANDLER and T. I. NIKOL'SKAYA, *Fiz. Met. Metall.* **32** (1971) 767.
8. N. C. PARSON and T. SHEPPARD, in "Proceedings of the 3rd International Conference on Al–Li Alloys", edited by C. Baker, P. J. Gregson. S. J. Harris and C. J. Peel (Institute of Metals, London, 1986) p. 222.
9. J. R. PICKENS, F. H. HEUBAUM, L. S. KRAMER and K. S. KUMAR, US Pat. 5032359, 16 July 1991.
10. J. J. WITTERS, E. W. LEE, W. B. LISAGOR, S. B. HERNER, R. J. KILMER and E. TALIA, in "Proceedings of the 6th International Conference on Al–Li Alloys", edited by M. Peters and P. J. Winkler (DGM Info., Oberursel, Germany, 1992) p. 351.
11. I. N. FRIDLYANDER, A. G. BRATUKHIN and V. G. DAVYDOV, *ibid.* p. 35.
12. S. F. BAUMANN and D. B. WILLIAMS, in " Proceedings of the 2nd International Conference on Al–Li Alloys", edited by T. H. Sanders and E. A. Starke (AIME, 1983) p. 17.
13. Y. BABA, *Trans. JIM* **13** (1972) 76.
14. I. J. POLMEAR and K. R. SARGANT, *Nature* **200** (1963) 669.
15. T. H. SANDERS, report no. NADC-76387-30, Naval Air Development Center, Warminster, PA (1976).
16. I. N. FRIDLYANDER, in "Proceedings of the 5th International Conference on Al–Li Alloys", edited by T. H. Sanders and E. A. Starke (MCE, 1989) p. 1359.
17. W. S. MILLER, A. J. CORNISH, A. P. TITCHENER and D. A. BENNETT, in "Proceedings of the 2nd International Conference on Al–Li Alloys", edited by T. H. Sanders and E. A. Starke (AIME, 1983) p. 335.
18. L. S. KRAMER, Unpublished Reasearch, Martin Marietta Laboratories, Baltimore, MD (1987).

19. S. J. HARRIS, B. NOBLE and K. DINSDALE in "Proceedings of the 2nd International Conference on Al–Li Alloys", edited by T. H. Sanders and E. A. Starke (AIME, 1983) p. 219.
20. L. A. KURTASOVA and POLYANSKII, *Fiz, Khim. Mekh. Mater* **13** (1977) 72.
21. P. NISKANEN, T. H. SANDERS Jr, M. MAREK and J. G. RINKER, in "Proceedings of the 1st International Conference on Al–Li Alloys", edited by T. H. Sanders and E. A. Starke (AIME, Warrendale, PA, 1981) p. 347.
22. A. LUO, D. J. LLOYD, A. GUPTA and W. V. YOUDELIS, *Acta Metall. Mater.* **41** (1993) 769.
23. T. V. SHCHEGOLEVA and O. F. RYBALKO, *Phys. Met. Metall.* **52** (1981) 120.

Received 9 November 1993
and accepted 16 May 1994